

Laser-Driven Multiferroics and Ultrafast Spin Current Generation

Masahiro Sato,^{1,2,3,4} Shintaro Takayoshi,⁵ and Takashi Oka^{6,7}

¹*Department of Physics, Ibaraki University, Mito, Ibaraki 310-8512, Japan*

²*Department of Physics and Mathematics, Aoyama-Gakuin University, Sagami-hara, Kanagawa 229-8558, Japan*

³*Advanced Science Research Center, Japan Atomic Energy Agency, Tokai, Ibaraki 319-1195, Japan*

⁴*ERATO, Japan Science and Technology Agency, Sendai, Miyagi 980-8577, Japan*

⁵*Department of Quantum Matter Physics, University of Geneva,*

24 quai Ernest-Ansermet, Geneva 1211, Switzerland

⁶*Max-Planck-Institut für Physik komplexer Systeme (MPI-PKS), Nöthnitzer Straße 38, Dresden 01187, Germany*

⁷*Max-Planck-Institut für Chemische Physik fester Stoffe (MPI-CPFS), Nöthnitzer Straße 40, Dresden 01187, Germany*

(Dated: March 4, 2024)

We propose an ultrafast way to generate spin chirality and spin current in a class of multiferroic magnets using a terahertz circularly polarized laser. Using the Floquet formalism for periodically driven systems, we show that it is possible to dynamically control the Dzyaloshinskii-Moriya interaction in materials with magnetoelectric coupling. This is supported by numerical calculations, by which additional resonant phenomena are found. Specifically, when a static magnetic field is applied in addition to the circularly polarized laser, a large resonant enhancement of spin chirality is observed resembling the electron spin resonance. Spin current is generated when the laser is spatially modulated by chiral plasmonic structures and could be detected using optospintronic devices.

PACS numbers: 75.85.+t, 75.10.Jm, 75.40.Gb, 71.70.Ej

Introduction.— Control of emergent collective phenomena by external fields is an important problem in condensed matter. Multiferroic magnets (for a review, see Refs. [1–3]) are opening new possibilities in this direction since the local spins are coupled not only to magnetic fields but to electric fields through the magnetoelectric (ME) coupling. Laser control of materials is attracting interest with a goal of realizing ultrafast and noncontact manipulation [4–14]. In the research community of magnetic systems, control of magnetism using a laser is being studied in the context of spin-pumping and spintronics [4–7]. On the other hand, in the field of electronic systems, periodically driven quantum systems draw the interest of many researchers. When the Hamiltonian is time periodic, the system can be described by the so-called Floquet states [15, 16], a temporal analog of the Bloch states, and it is possible to control their quantum nature. For noninteracting systems, the control of the band topology has been studied theoretically [8–10] and experimentally [13, 14]. It is possible to understand the effect of a laser through a mapping from the time-dependent Hamiltonian to a *static* effective Hamiltonian using the Floquet theory, and the change of quantum state, e.g., topology and symmetry, is attributed to the emergent terms in the static effective Hamiltonian. This framework can also be applied to quantum magnets. Laser-induced magnetization growth in general quantum magnets [17, 18] as well as laser-driven topological spin states [18, 19], a quantum spin versions of Floquet topological insulators, were proposed recently.

In the current work, we apply the Floquet theory to quantum *multiferroics* and study the synthetic interactions appearing in the effective Floquet Hamiltonian [see Eq. (3)]. We show that when elliptically or circularly po-

larized lasers are applied, an additional Dzyaloshinskii-Moriya (DM) interaction [20] emerges and its direction (DM vector) can be controlled. The DM interaction generally favors a spiral magnetic order and if its strength is spatially modulated, it is possible to induce spin currents. Through direct numerical calculations, we verify this picture, and then propose a way to generate ultrafast spin currents in a realistic device by optical means.

Multiferroics with laser application.— In multiferroics [1–3], spin degrees of freedom couple to electromagnetic waves not only through the Zeeman coupling, but also through the ME coupling. This is because the local polarization vector is related to spin degrees of freedom from crystallographic reasons. The Hamiltonian for multiferroics subject to a laser can be expressed as

$$\mathcal{H}(t) = \mathcal{H}_0 + \mathcal{H}_E(t) + \mathcal{H}_B(t), \quad (1)$$

where \mathcal{H}_0 is the spin Hamiltonian, and the laser-driven time-dependent terms $\mathcal{H}_E(t) = -\mathbf{E}(t) \cdot \mathbf{P}$ and $\mathcal{H}_B(t) = -g\mu_B \mathbf{B}(t) \cdot \mathbf{S}$ respectively denote the ME coupling of the total polarization \mathbf{P} with electric field $\mathbf{E}(t)$, and the Zeeman coupling between the total spin \mathbf{S} with the magnetic field $\mathbf{B}(t)$ (g is Landé’s g factor and μ_B is Bohr magneton). The polarization \mathbf{P} is given by a function of spin operators. Electric and magnetic components of the laser are represented as $\mathbf{E}(t) = E_0(\cos(\Omega t + \delta), -\sin(\Omega t), 0)$ and $\mathbf{B}(t) = E_0 c^{-1}(-\sin(\Omega t), -\cos(\Omega t + \delta), 0)$, respectively. The value of δ fixes the helicity of the laser, i.e., $\delta = 0, \pi$, and $\pi/2$ respectively corresponds to right-circularly, left-circularly, and linearly polarized lasers. Symbols Ω and c stand for the laser frequency and the speed of light, respectively.

Synthetic interactions from Floquet theory.— We apply the Floquet theory and the Ω^{-1} expansion to Eq. (1).

From the discrete Fourier transform of the time-periodic Hamiltonian, $\mathcal{H}(t) = \sum_m e^{-im\Omega t} H_m$ (m : integer), the static effective Hamiltonian $\mathcal{H}_{\text{eff}} = \sum_{i \geq 0} \Omega^{-i} \mathcal{H}_{\text{eff}}^{(i)}$ can be expanded in terms of Ω^{-1} and the leading two terms are given by [21–23]

$$\mathcal{H}_{\text{eff}}^{(0)} = H_0, \quad \mathcal{H}_{\text{eff}}^{(1)} = - \sum_{m>0} [H_{+m}, H_{-m}] / m. \quad (2)$$

For large enough Ω , we can truncate \mathcal{H}_{eff} up to the Ω^{-1} order. In the present multiferroic system, the first correction $\mathcal{H}_{\text{eff}}^{(1)}$, which we call the synthetic interaction, is given by

$$\begin{aligned} \mathcal{H}_{\text{syn}} \equiv \Omega^{-1} \mathcal{H}_{\text{eff}}^{(1)} = & -\frac{i \cos \delta}{2\Omega} \{ \alpha^2 [\tilde{P}^x, \tilde{P}^y] \\ & + \alpha \beta ([\tilde{P}^x, S^x] + [\tilde{P}^y, S^y]) + \beta^2 [S^x, S^y] \} \end{aligned} \quad (3)$$

with $\alpha = g_{\text{me}} E_0$, and $\beta = g \mu_B E_0 c^{-1}$. Here, g_{me} is the ME coupling constant [see Eq. (4)] with $\tilde{\mathbf{P}}$ being a dimensionless function of spins, i.e., $\mathbf{P} = g_{\text{me}} \tilde{\mathbf{P}}$. Let us comment on the magnitude of the synthetic terms. The strongest magnetic field β of a terahertz (THz) laser attains 1–10 T [24, 25]. The magnitude of $g_{\text{me}}(\Omega)$ can be large in a gigahertz (GHz) to THz region [26, 27], and from both experimental and theoretical analyses [26–29], the value of α is expected to be of the same order as β . If we use as reference the typical value of exchange coupling $J = 0.1$ –10 meV (~ 1 –100 T) in standard magnets (e.g., XXZ magnets in Eq. (7)) both α/J and β/J can achieve values of 0.1–1.

The precise form of the synthetic interaction depends on the type of the ME coupling. Here we consider the case where the polarization $\mathbf{P} = \sum_{\mathbf{r}, \mathbf{r}'} \mathbf{P}_{\mathbf{r}, \mathbf{r}'}$ is given by a product of two spin operators on sites $(\mathbf{r}, \mathbf{r}')$. $\mathbf{P}_{\mathbf{r}, \mathbf{r}'}$ is proportional to the exchange interaction (energy density) $\mathbf{S}_{\mathbf{r}} \cdot \mathbf{S}_{\mathbf{r}'}$ in symmetric magnetostriction type multiferroics [30], while it is proportional to the vector spin chirality $\mathbf{S}_{\mathbf{r}} \times \mathbf{S}_{\mathbf{r}'}$ in the antisymmetric magnetostriction type (also known as the inverse DM effect) [28, 31–34]. The term $[\tilde{P}^x, \tilde{P}^y]$ thereby yields three spin terms such as the scalar spin chirality. In Ref. 19, it was shown that a three-spin term related to the scalar spin chirality is generated in the symmetric ME coupling case and can induce a topological gap in spin liquids. In addition, $[\tilde{P}^a, S^b]$ and $[S^x, S^y]$ induce two-spin and single-spin terms, respectively.

Two-spin system.— To illustrate the effect of Eq. (3), let us first focus on a simple two-spin multiferroic model depicted in Fig. 1(a). The applied laser travels toward the $-z$ direction, and the two-spin multiferroic magnet is within the xy plane. We assume that the two-spin system $\mathbf{S}_{1,2}$ possesses an electric polarization \mathbf{P} through the ME coupling as

$$\mathbf{P} = g_{\text{me}} \mathbf{e}_{12} \times (\mathbf{S}_1 \times \mathbf{S}_2), \quad (4)$$

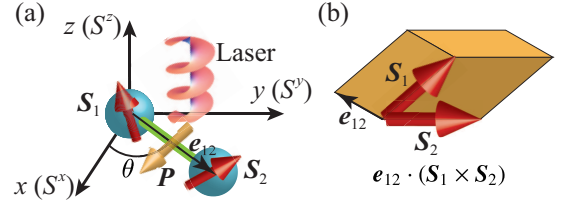


FIG. 1: (a) Schematic picture of a multiferroic system consisting of two spins $\mathbf{S}_{1,2}$ in a circularly polarized laser. The vector \mathbf{P} represents the electric polarization. (b) Schematic picture for geometric meaning of the synthetic DM interaction in Eq. (5).

where $\mathbf{e}_{12} = (\cos \theta, \sin \theta, 0)$ is the vector connecting two spins (the distance between spins is set to unity). This ME coupling is known to be responsible for electric polarization in a wide class of spiral ordered (i.e., chirality ordered) multiferroic magnets [1–3, 32–34]. Using Eq. (3), we obtain the synthetic interaction

$$\mathcal{H}_{\text{syn}} = \frac{\alpha \beta}{2\Omega} \cos \delta (\mathbf{e}_{12} \cdot \mathbf{V}_{12}) + \frac{\beta^2}{2\Omega} \cos \delta (S_1^z + S_2^z), \quad (5)$$

where $\mathbf{V}_{12} = \mathbf{S}_1 \times \mathbf{S}_2$ is the vector spin chirality. The first term is the laser-driven DM interaction and generated via the single-photon absorption and emission as shown in Ref. 21. This DM term is geometrically illustrated by the volume of a parallelepiped as in Fig. 1(b). The three spin term from $[\tilde{P}^x, \tilde{P}^y]$ disappears in Eq. (5) since \mathbf{e}_{12} is within the polarization plane.

The result (5) is valid for any spin Hamiltonian \mathcal{H}_0 with arbitrary spin magnitude S . In the original model (1), the DM vector in $\mathbf{E}(t) \cdot \mathbf{P}$ is parallel to z axis. On the other hand, Eq. (5) shows that the synthetic DM vector is in the direction of \mathbf{e}_{12} , which is in the xy plane and perpendicular to the z axis. The coefficient $\alpha \beta$ in Eq. (5) indicates that both ME and Zeeman terms are necessary for emergence of the synthetic DM interaction. It is also significant that the laser should be circularly or elliptically polarized. In fact, \mathcal{H}_{syn} vanishes when the laser is linearly polarized ($\delta = \pi/2$). We emphasize that the synthetic DM coupling constant and its sign can be controlled by changing the laser helicity.

We comment on the importance of breaking the SU(2) symmetry of the system. If the spin Hamiltonian \mathcal{H}_0 is spin-rotationally [i.e., SU(2)] symmetric, the Zeeman term $\mathcal{H}_B(t)$ commutes with \mathcal{H}_0 . This means that the laser-driven β term plays no role in the growth of spin chirality. Thus, it is important that the system has magnetic anisotropy or spontaneous symmetry breakdown that relaxes the SU(2) symmetry.

Many-spin system (spirals and chiral-solitons).— It is straightforward to extend our result (5) to multiferroic magnets consisting of many spins. For instance, the static effective Hamiltonian for an 1D multiferroic spin chain \mathcal{H}_0^{1D} along the x axis ($\theta = 0$) with a circularly

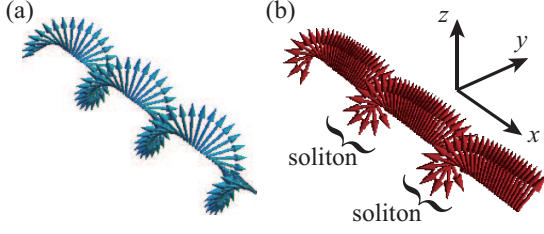


FIG. 2: (a) Spin spiral (helical) ordered state and (b) chiral-soliton-lattice state can be laser-induced if the exchange coupling is AF and FM, respectively.

polarized laser is given by

$$\mathcal{H}_{\text{eff}}^{\text{1D}} = \mathcal{H}_0^{\text{1D}} \pm \sum_j \frac{\alpha\beta}{2\Omega} \mathcal{V}_{j,j+1}^x \pm \sum_j \frac{\beta^2}{2\Omega} S_j^z, \quad (6)$$

where $\mathcal{V}_{j,j+1} \equiv \mathbf{S}_j \times \mathbf{S}_{j+1}$, and the sign \pm respectively corresponds to $\delta = 0$ and π . Here we assume that the bond polarization $\mathbf{P}_{j,j+1}$ is proportional to the bond chirality $\mathcal{V}_{j,j+1}$, and the total polarization is given by $\mathbf{P}_{\text{tot}} = g_{\text{me}} \sum_j \mathbf{e}_{j,j+1} \times \mathcal{V}_{j,j+1}$ ($\mathbf{e}_{j,j+1}$ stands for a vector connecting the spin site j and $j+1$).

The effective model (6) is known to support interesting spin states with spatial modulations if the interaction in $\mathcal{H}_0^{\text{1D}}$ is short ranged. A spin spiral state [Fig. 2(a)] emerges when the exchange is antiferromagnetic (AF) due to the competition between exchange and laser-induced DM interaction. On the other hand, in the case of a ferromagnetic exchange, it is known that competition among exchange, DM and Zeeman couplings can lead to a chiral-soliton-lattice state [Fig. 2(b)] [35, 36] as the classical ground state of $\mathcal{H}_{\text{eff}}^{\text{1D}}$. This indicates that a laser can create several types of spiral spin textures depending on lattices and interactions of the multiferroic system \mathcal{H}_0 .

Numerical analysis.— The Floquet effective Hamiltonian and the predicted emergence of the synthetic interaction (3) are the general result and apply to a broad class of multiferroics. However, there are limitations to the theory: (i) The effective Hamiltonian is applicable when the driving frequency (=photon energy) Ω is much larger than all the other energy scales in the system, and (ii) when many-body interactions are present, the system eventually heats up [37, 38]. As a complementary test, we use a numerical approach and perform direct time dependent calculations in a laser-driven multiferroic model based on $\mathcal{H}(t)$ (1). Here, we focus on simple multiferroic XXZ spin- $\frac{1}{2}$ chains aligned in the x direction ($\theta = 0$) with an external magnetic field H

$$\mathcal{H}_0^{\text{1D}} = \mathcal{H}_{\text{XXZ}} = \sum_j (J \mathbf{S}_j \cdot \mathbf{S}_{j+1} - J\Delta S_j^x S_{j+1}^x - H S_j^x). \quad (7)$$

In order to break the SU(2) symmetry, we introduced either an Ising anisotropy $-J\Delta S_j^x S_{j+1}^x$ or a static Zeeman

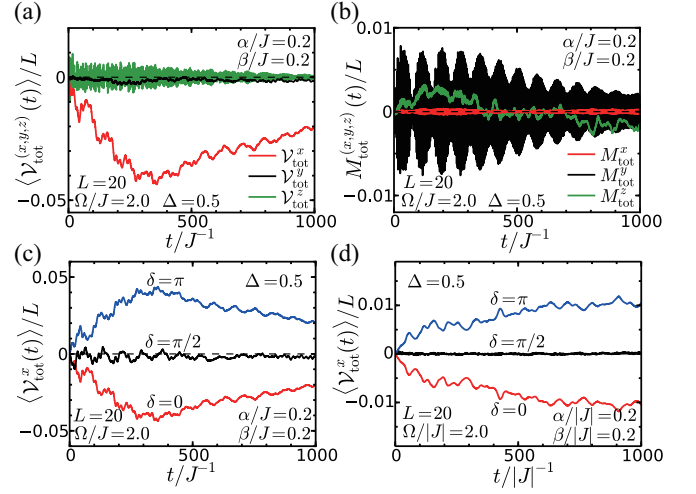


FIG. 3: Simulation results of a multiferroic XXZ chain ($\Delta = 0.5$, $H/J = 0$) in a circularly polarized laser. Time evolutions of (a) vector chirality ($\langle \mathcal{V}_{\text{tot}}(t) \rangle$) and (b) magnetization $\mathbf{M}_{\text{tot}}(t)$ in an AF XXZ model under a circularly polarized laser ($J > 0$ and $\delta = 0$). (c) Laser helicity (δ) dependence of ($\langle \mathcal{V}_{\text{tot}}^x(t) \rangle$). (d) Time evolution of vector chirality in the case of a ferromagnetic exchange ($J < 0$).

term $-HS_j^x$. In the case of circularly polarized laser with $\delta = 0$ ($\delta = \pi$), the effective Hamiltonian Eq. (6) predicts the emergence of x component of vector chirality ($\langle \mathcal{V}_{\text{tot}}^x \rangle < 0$ (> 0)).

We perform simulations for finite-size systems with L spins. The initial state is set to the ground state of Eq. (7) obtained by numerical diagonalization. The laser is turned on at $t = 0$ and the system evolves according to the time-dependent Hamiltonian $\mathcal{H}(t)$ (1). The time evolution of the state $|\Psi(t)\rangle$ is obtained by integrating the Schrödinger equation $i(d/dt)|\Psi(t)\rangle = \mathcal{H}(t)|\Psi(t)\rangle$ using the fifth order Runge-Kutta method. In the numerical analysis below, we set $\alpha/J = \beta/J = 0.2$.

First, consider the case of $\Delta = 0.5$ and $H = 0$. In Figs. 3(a) and 3(b), we plot the typical time evolutions of vector chirality $\langle \mathcal{V}_{\text{tot}}(t) \rangle = \langle \sum_j \mathcal{V}_{j,j+1}(t) \rangle$ and magnetization $\mathbf{M}_{\text{tot}}(t) = \langle \sum_j \mathbf{S}_j(t) \rangle$ for an XXZ model with $H = 0$ in a circularly polarized laser with $\Omega/J = 2$ and $\delta = 0$. The vector chirality $\langle \mathcal{V}_{\text{tot}}^x(t) \rangle < 0$ appears as expected while $\langle \mathcal{V}_{\text{tot}}^{(y,z)}(t) \rangle$ remains small. The dependence of the vector chirality on the laser helicity δ is depicted in Figs. 3(c) and 3(d). We see that $\langle \mathcal{V}_{\text{tot}}^x(t) \rangle$ becomes negative (positive) for $\delta = 0$ (π), while it remains very small for linear polarization $\delta = \pi/2$. These behaviors are consistent with the prediction (6) from the Floquet theory. However, the vector chirality does not keep on growing but becomes saturated around $t/J^{-1} \sim 400$ in Fig. 3(c). This may be due to heating; the system's “effective temperature” exceeds the magnitude of the synthetic term ($\sim \alpha\beta/\Omega$) around this time, and the linear growth of the chirality stops. This is consistent with re-

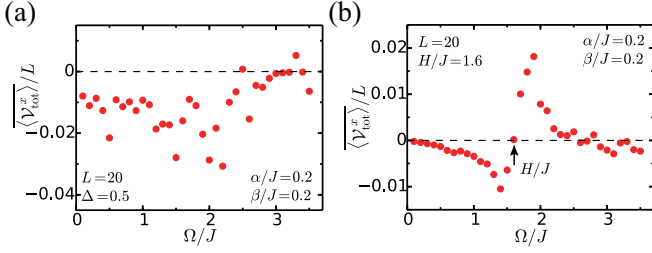


FIG. 4: Ω dependence of time average of vector chirality $\overline{\langle \mathbf{V}_{\text{tot}}^x \rangle}$ in (a) AF ($J > 0$) XXZ model without external magnetic field and (b) Heisenberg model ($\Delta = 0$) with external magnetic field. Around $\Omega = H$, we observe a large magnitude of laser-driven chirality due to a resonant behavior.

cent studies on “heating” in closed periodically driven systems that have revealed that the effective Hamiltonian approach, e.g., Eq. (6), is valid only for finite time, and if the driving is continued the system will approach an infinite temperature state [37, 38]. When the system is coupled to a heat reservoir, the heating can be stopped and the system can be stabilized [12]. Figure 3(b) shows that the magnetization $\mathbf{M}_{\text{tot}}(t)$ does not grow but only exhibits an oscillation with small amplitude.

In order to understand how the induced chirality depends on the laser frequency Ω , we define its time average as

$$\overline{\langle \mathbf{V}_{\text{tot}} \rangle} \equiv \frac{1}{T} \int_0^T dt \langle \mathbf{V}_{\text{tot}}(t) \rangle \quad (8)$$

with $T = 1000J^{-1}$. As shown in Fig. 4(a), for the XXZ chain in zero field, the induced chirality is typically negative, which agrees with the prediction from the Floquet effective Hamiltonian (6), but since Eq. (6) is based on the high frequency expansion, it fails to explain the detailed structure in the simulation. We find many small peaks in Fig. 4(a) that are presumably due to resonance with many-body excited states.

We also consider laser-driven spin chains in a static magnetic field. Naively, we may expect that the magnetic field will play the same role as the Ising anisotropy, i.e., a source to break the $SU(2)$ symmetry, and no qualitative difference would occur. However, in Fig. 4(b), the result of direct calculation shows a resonant behavior in the generation of a vector chirality around $\Omega \sim H$, which is clearly not described by the effective Hamiltonian (6). We verified that a similar resonant behavior also occurs in a multiferroic spin-1 chain and a spin- $\frac{1}{2}$ ladder (see Supplemental Material [21]), which indicates that the resonance around $\Omega \sim H$ is universal in a broad class of multiferroic systems. What happens around $\Omega \sim H$ is analogous to electron spin resonance (ESR). Thus, our calculation implies that by using circularly polarized laser in an ESR setup, it is possible to efficiently generate a vector chirality in multiferroics.

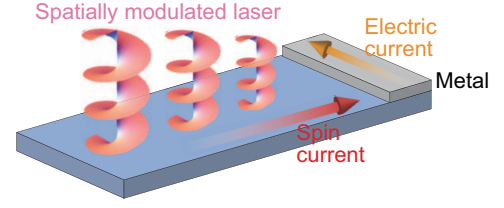


FIG. 5: Setup to detect signatures of laser-driven DM interactions by measuring spin current. The spin current pumped from a spin chain to a metal with a strong spin-orbit coupling is changed into an electric current via inverse spin Hall effect in the metal.

Detection schemes.— Finally, we propose schemes to detect the synthetic DM interaction and vector chirality. Detection using pump-probe optical methods is in principle possible by observing nontrivial textures, e.g., spiral states [21]. Another scheme is to utilize optospinronic methods with plasmon resonances proposed in Ref. [39]. The underlying idea is to apply a *spatially modulated* circularly polarized laser to a multiferroic magnet (Fig. 5). Assuming that the exchange coupling is dominant in the time-dependent Hamiltonian of the spin chain $\mathcal{H}_{\text{XXZ}} + \mathcal{H}_E(t) + \mathcal{H}_B(t)$, the Heisenberg equation of motion shows that

$$i(dS_j^x/dt) \approx [S_j^x, \mathcal{H}_{\text{XXZ}}] = iJ(\mathcal{V}_{j-1,j}^x - \mathcal{V}_{j,j+1}^x). \quad (9)$$

Similar expressions hold for higher dimensions and therefore a finite spin current $\langle dS_j^x/dt \rangle$ appears due to a site-dependent vector chirality if the laser is spatially modulated. A circularly polarized laser with large spatial modulation can be realized in the near field of chiral plasmonic structures [40]. Then, in order to detect the spin current, one needs to combine the plasmonic structure with a metallic electrode where the spin current is transformed into an electric current by inverse spin Hall effect [41–44]. The spin current is injected from the multiferroic magnet to the electrode if $\langle dS_j^x/dt \rangle$ is nonzero at the interface [45, 46]. Using materials with strong spin-orbit coupling such as Pt [44] for the electrode, we can observe the generation of a laser-driven chirality through an electric voltage drop. In the Supplemental Material [21], we numerically show that an inhomogeneous chirality appears when we apply a spatially modulated laser.

Distinction of mechanisms is an important issue. In contrast with other effects of laser such as heating, the laser-driven DM interaction strongly depends on the direction of the laser as can be seen from Fig. 1 and Eq. (4), and thus systematic measurements with sample rotation are useful for making clear the origin.

Summary.— In conclusion, we proposed a way to generate and control DM interactions and spin currents in multiferroics utilizing elliptically polarized lasers. Our understanding is based on the Floquet theory with the Ω^{-1} expansion, which captures the general tendency of

the numerical results, while we find an additional resonant enhancement of spin chirality when a static magnetic field is applied.

We would like to thank Hidekazu Misawa, Yuichi Ohnuma, Stephan Kaiser, Thomas Weiss and Shin Miyahara for fruitful discussions. M.S. is supported by KAKENHI (Grants No. 26870559, No. 25287088, and No. 15H02117), S.T. by the Swiss NSF under Division II, and T.O. by KAKENHI (Grant No. 23740260 and No. 15H02117). S.T. and T.O. are also supported by ImPact project (No. 2015-PM12-05-01) from JST.

-
- [1] Y. Tokura, S. Seki, and N. Nagaosa, Rep. Prog. Phys. **77**, 076501 (2014).
 - [2] Y. Tokura, and S. Seki, Adv. Mat. **22**, 1554 (2010).
 - [3] K. F. Wang, J.-M. Liu, and Z. F. Ren, Adv. Phys. **58**, 321 (2009).
 - [4] A. Kirilyuk, A. V. Kimel, and T. Rasing, Rev. Mod. Phys. **82**, 2731 (2010).
 - [5] C. Vicario, C. Ruchert, F. Ardana-Lamas, P. M. Derlet, B. Tudu, J. Luning, and C. P. Hauri, Nat. Photon. **7**, 720 (2013).
 - [6] A. J. Schellekens, K.C. Kuiper, R. R. J. C. de Wit, and B. Koopmans, Nat. Commun. **5**, 4333 (2014).
 - [7] G. Choi, B. Min, K. Lee and D. G. Cahill, Nat. Commun. **5**, 4334 (2014).
 - [8] T. Oka and H. Aoki, Phys. Rev. B **79**, 081406(R) (2009).
 - [9] T. Kitagawa, T. Oka, A. Brataas, L. Fu, and E. Demler, Phys. Rev. B **84**, 235108 (2011).
 - [10] N. H. Lindner, G. Refael, and V. Galitski, Nat. Phys. **7**, 490 (2011).
 - [11] N. Tsuji, T. Oka, and H. Aoki, Phys. Rev. B **78**, 235124 (2008).
 - [12] N. Tsuji, T. Oka, and H. Aoki, Phys. Rev. Lett. **103**, 047403 (2009).
 - [13] Y. H. Wang, H. Steinberg, P. Jarillo-Herrero, and N. Gedik, Science **342**, 453 (2013).
 - [14] G. Jotzu, M. Messer, Rémi Desbuquois, M. Lebrat, T. Uehlinger, D. Greif, and T. Esslinger, Nature (London) **515**, 237 (2014).
 - [15] J. H. Shirley, Phys. Rev. **138**, B979 (1965).
 - [16] H. Sambe, Phys. Rev. A **7**, 2203 (1973).
 - [17] S. Takayoshi, H. Aoki, and T. Oka, Phys. Rev. B **90**, 085150 (2014).
 - [18] S. Takayoshi, M. Sato, and T. Oka, Phys. Rev. B **90**, 214413 (2014).
 - [19] M. Sato, Y. Sasaki, and T. Oka, [arXiv:1404.2010](https://arxiv.org/abs/1404.2010).
 - [20] I. Dzyaloshinsky, J. Phys. Chem. Solids **4**, 241 (1958); T. Moriya, Phys. Rev. **120**, 91 (1960).
 - [21] See Supplemental Material.
 - [22] F. Casas, J. A. Oteo, and J. Ros, J. Phys. A **34**, 3379 (2001).
 - [23] E. S. Mananga and T. Charpentier, J. Chem. Phys. **135**, 044109 (2011).
 - [24] H. Hirori, K. Shinokita, M. Shirai, S. Tani, Y. Kadoya, and K. Tanaka, Nat. Commun. **2**, 594 (2011).
 - [25] A. Pashkin, F. Junginger, B. Mayer, C. Schmidt, O. Schubert, D. Brida, R. Huber, and A. Leitenstorfer, IEEE J. Sel. Topics Quant. Electr. **19**, 8401608 (2013).
 - [26] Y. Takahashi, R. Shimano, Y. Kaneko, H. Murakawa, and Y. Tokura, Nat. Phys. **8**, 121 (2012).
 - [27] D. Hvonen, U. Nagel, T. Rm, Y. J. Choi, C. L. Zhang, S. Park, and S.-W. Cheong, Phys. Rev. B **80**, 100402(R) (2009).
 - [28] H. Katsura, A. V. Balatsky, and N. Nagaosa, Phys. Rev. Lett. **98**, 027203 (2007).
 - [29] S. Furukawa, M. Sato, and S. Onoda, Phys. Rev. Lett. **105**, 257205 (2010).
 - [30] T. Moriya, J. Phys. Soc. Jpn. **23**, 490 (1967); J. App. Phys. **39**, 1042 (1968).
 - [31] Y. Tanabe, T. Moriya, and S. Sugano, Phys. Rev. Lett. **15**, 1023 (1965).
 - [32] H. Katsura, N. Nagaosa, and A. V. Balatsky, Phys. Rev. Lett. **95**, 057205 (2005).
 - [33] M. Mostovoy, Phys. Rev. Lett. **96**, 067601 (2006).
 - [34] I.A. Sergienko and E. Dagotto, Phys. Rev. B **73**, 094434 (2006).
 - [35] J. Kishine, K. Inoue, and Y. Yoshida, Prog. Theo. Phys. Suppl. **159**, 82 (2005).
 - [36] Y. Togawa, Y. Kousaka, S. Nishihara, K. Inoue, J. Akimitsu, A. S. Ovchinnikov, and J. Kishine, Phys. Rev. Lett. **111**, 197204 (2013).
 - [37] L. D'Alessio and M. Rigol, Phys. Rev. X **4**, 041048 (2014).
 - [38] A. Lazarides, A. Das, and R. Moessner, Phys. Rev. E **90**, 012110 (2014).
 - [39] K. Uchida, H. Adachi, T. Kikkawa, S. Ito, Z. Qiu, S. Maekawa, and E. Saitoh, Nat. Commun. **6**, 5910 (2015).
 - [40] M. Schferling, D. Dregely, M. Hentschel, and H. Giessen, Phys. Rev. X **2**, 031010 (2012).
 - [41] E. Saitoh, M. Ueda, H. Miyajima, and G. Tatara, App. Phys. Lett. **88**, 182509 (2006).
 - [42] S. O. Valenzuela and M. Tinkham, Nature (London) **442**, 176 (2006).
 - [43] *Spin Current*, edited by S. Maekawa, S. O. Valenzuela, E. Saitoh and T. Kimura (Oxford University Press, Oxford, England, 2012).
 - [44] K. Uchida, H. Adachi, T. Kikkawa, A. Kirihaara, M. Ishida, S. Yorozu, S. Maekawa, and E. Saitoh, Proc. IEEE **99**, 1 (2016).
 - [45] Y. Tserkovnyak, A. Brataas, and G. E. W. Bauer, Phys. Rev. Lett. **88**, 117601 (2002).
 - [46] H. Adachi, K. Uchida, E. Saitoh and S. Maekawa, Rep. Prog. Phys. **76**, 036501 (2013).

Supplemental Material

S1. Floquet theorem and Ω^{-1} expansion

Here, we explain the Floquet theorem and the Ω^{-1} expansion scheme of the effective Hamiltonian in relation with Eqs. (2), (3), and (5) in the main text. This theorem can be viewed as time version of Bloch theorem [1] for quantum systems with spatially periodicity (such as crystals).

We consider a time-dependent Schrödinger equation

$$i\frac{\partial}{\partial t}|\Psi(t)\rangle = \mathcal{H}(t)|\Psi(t)\rangle. \quad (\text{S1})$$

for a time-periodic system $\mathcal{H}(t) = \mathcal{H}(t + T)$. We perform discrete Fourier transform for the Hamiltonian $\mathcal{H}(t) = \sum_m e^{-im\Omega t} H_m$ where the frequency Ω is $2\pi/T$, and m is an integer running from $-\infty$ to ∞ . The solution can be written as $|\Psi(t)\rangle = e^{-i\epsilon t}|\Phi(t)\rangle$ where $|\Phi(t)\rangle$ is the Floquet state, which is periodic in time, i.e., $|\Phi(t)\rangle = |\Phi(t + T)\rangle$, and ϵ is the Floquet quasienergy. The Floquet state can be expanded as $|\Phi(t)\rangle = \sum_m e^{-im\Omega t}|\Phi^m\rangle$. Substituting this to Eq. (S1), we obtain the following eigenvalue equations

$$\sum_m (H_{n-m} - m\Omega\delta_{mn})|\Phi^m\rangle = \epsilon|\Phi^n\rangle. \quad (\text{S2})$$

In the model studied in the main text, nonzero components are only time-independent part and terms proportional to $\exp(\pm i\Omega t)$, hence we can rewrite Eq. (S2) in the following matrix form:

$$\begin{pmatrix} \ddots & & & & & \\ & H_0 - 2\Omega & H_{+1} & 0 & 0 & 0 \\ & H_{-1} & H_0 - \Omega & H_{+1} & 0 & 0 \\ & 0 & H_{-1} & H_0 & H_{+1} & 0 \\ & 0 & 0 & H_{-1} & H_0 + \Omega & H_{+1} \\ & 0 & 0 & 0 & H_{-1} & H_0 + 2\Omega \\ & & & & & \ddots \end{pmatrix} \begin{pmatrix} \vdots \\ |\Phi^2\rangle \\ |\Phi^1\rangle \\ |\Phi^0\rangle \\ |\Phi^{-1}\rangle \\ |\Phi^{-2}\rangle \\ \vdots \end{pmatrix} = \epsilon \begin{pmatrix} \vdots \\ |\Phi^2\rangle \\ |\Phi^1\rangle \\ |\Phi^0\rangle \\ |\Phi^{-1}\rangle \\ |\Phi^{-2}\rangle \\ \vdots \end{pmatrix}. \quad (\text{S3})$$

The block structure appearing in Eqs. (S2) and (S3) is understood intuitively as “photon dressed states”. The frequency Ω is interpreted as a photon energy, and thereby $|\Phi^{-m}\rangle$ is regarded as a state in Hilbert subspace with m photons. This can also be seen from the energy shift $m\Omega$ in the diagonal components of Eq. (S3). Different subspaces are hybridized by H_{+1} and H_{-1} , which correspond to photon emission and absorption processes, respectively. In general, $H_{\pm m}$ represents direct multi-photon processes. Figure S1 illustrates the hybridization structure of the Floquet system, where a step in the Floquet direction corresponds to increase or decrease of photon energy.

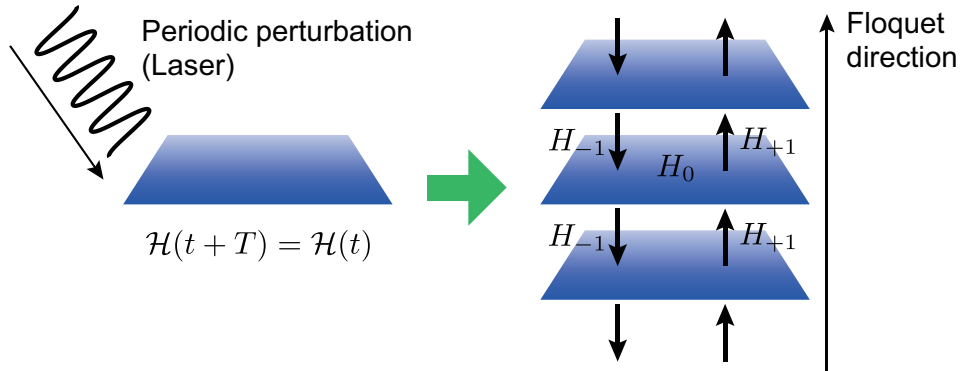


FIG. S1: A system with time-periodic perturbation (left) is mapped to the Floquet eigenvalue problem (right). The latter corresponds to a system consisting of subspaces with different photon number (Floquet direction) coupled with each other through the off-diagonal components H_m ($m \neq 0$) of the Floquet Hamiltonian.

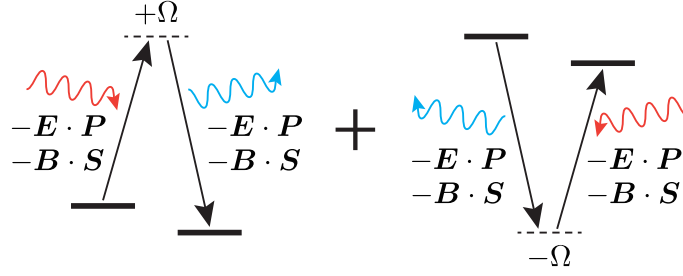


FIG. S2: Terms in the effective Hamiltonian (S7) is considered as photon absorption-emission and emission-absorption processes.

The infinite-dimensional eigenvalue problem Eq. (S3) can be reduced to a finite-dimensional problem using a Ω^{-1} expansion. If we focus on the zero photon subspace $|\Phi^0\rangle$, the neighboring subspaces $|\Phi^{\pm 1}\rangle$ become energetically far in the large Ω limit. The lowest order correction due to the off-diagonal terms $H_{\pm 1}$ is to simply induce virtual photon absorption-emission or emission-absorption processes which result in an effective Hamiltonian [2]

$$\mathcal{H}_{\text{eff}} = H_0 - [H_{+1}, H_{-1}]/\Omega + \mathcal{O}(1/\Omega^2). \quad (\text{S4})$$

This corresponds to Eq. (2) in the main text. Beyond the first order correction, either the Floquet-Magnus expansion or the Brillouin-Wigner perturbation can be applied. The comparison of these methods are given in Ref. [3].

As for the model considered in the main text, the virtual photon processes can be visualized as in Fig. S2. Let us apply this Ω^{-1} expansion scheme for our laser-driven system. In the two-spin system in Fig. 1(a) of the main text, time-dependent laser-driven terms are expressed as

$$\mathcal{H}_E(t) = -\mathbf{E}(t) \cdot \mathbf{P} = -\alpha[\sin\theta \cos(\Omega t + \delta)\mathcal{V}_{12}^z + \cos\theta \sin(\Omega t)\mathcal{V}_{12}^z], \quad (\text{S5})$$

$$\mathcal{H}_B(t) = -g\mu_B \mathbf{B}(t) \cdot (\mathbf{S}_1 + \mathbf{S}_2) = \beta[\sin(\Omega t)(S_1^x + S_2^x) + \cos(\Omega t + \delta)(S_1^y + S_2^y)], \quad (\text{S6})$$

where $\alpha = g_{\text{me}}E_0$ and $\beta = g\mu_B E_0 c^{-1}$. Using this expression, we can easily compute the commutator $[H_{+1}, H_{-1}]$ and then we obtain Eq. (5) in the main text,

$$\mathcal{H}_{\text{syn}} = \frac{\alpha\beta}{2\Omega} \cos\delta(\mathbf{e}_{12} \cdot \mathbf{V}_{12}) + \frac{\beta^2}{2\Omega} \cos\delta(S_1^z + S_2^z). \quad (\text{S7})$$

S2. Resonant-like phenomena in laser-driven multiferroic spin models

In the main text, we showed that a resonant phenomenon occurs in laser-driven multiferroic spin- $\frac{1}{2}$ chain in a static Zeeman magnetic field H with resonant frequencies around $\Omega = H$ [Fig. 4(b)]. In this section, in order to show that this resonance is not a special feature of a particular model, we numerically investigate laser-induced vector chirality in two other models: a spin-1 Heisenberg chain and a two-leg spin- $\frac{1}{2}$ ladder in circularly polarized laser with $\delta = 0$. We assume an antisymmetric magnetostriction type ME coupling in these two models as in the model in the main text. The Hamiltonian of the spin-1 chain is given by the same form as Eq. (7) with replacing spin- $\frac{1}{2}$ operators with spin-1 ones, while that of the spin- $\frac{1}{2}$ ladder is

$$\begin{aligned} \mathcal{H}_{\text{lad}} = & J \sum_{n=1,2} \sum_j (\mathbf{S}_{n,j} \cdot \mathbf{S}_{n,j+1} - \Delta S_{n,j}^x S_{n,j+1}^x) + J_{\perp} \sum_j (\mathbf{S}_{1,j} \cdot \mathbf{S}_{2,j} - \Delta S_{1,j}^x S_{2,j+1}^x) \\ & - H \sum_{n=1,2} \sum_j S_{n,j}^x \\ & - g_{\text{me}} \mathbf{E}(t) \cdot \sum_{n=1,2} \sum_j \mathbf{e}_{j,j+1} \times \mathbf{V}_{n,j,j+1} - g\mu_B \mathbf{B}(t) \cdot \sum_{n=1,2} \sum_j \mathbf{S}_{n,j}, \end{aligned} \quad (\text{S8})$$

where n and j denote the leg and rung indices, respectively. The first and second terms are respectively leg (J) and rung (J_{\perp}) exchange couplings, and third is the Zeeman interaction of static external field H . The legs of the ladder are situated along the x direction. The final line $\mathcal{H}_{\text{laser}}(t)$ is the laser-driven time-dependent interaction, and

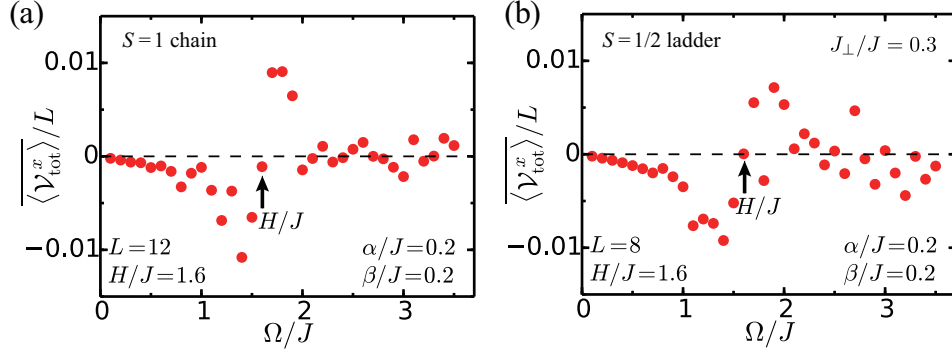


FIG. S3: Time-averaged vector chirality in laser-driven multiferroic spin-1 chain (a) and spin- $\frac{1}{2}$ ladder (b). In both the systems, resonant peaks appear just below and above $\Omega = H$. We choose the numerically obtained ground states of the two models as the initial states at $t = 0$. We set $\Delta = 0$ (no XXZ anisotropy), $H/J = 1.6$, and $J_{\perp}/J = 0.3$. The system size L means the total number of sites along chain and leg directions.

$\mathcal{V}_{n,j,j+1} = \mathbf{S}_{n,j} \times \mathbf{S}_{n,j+1}$ is the n -th chain vector chirality. We assume that the ME coupling exists only on the leg bonds (not rung). The explicit form of the laser-driven term is the following:

$$\begin{aligned} \mathcal{H}_{\text{laser}}(t) &= -g_{\text{me}} E_0 \sin(\Omega t) \sum_{n=1,2} \sum_j \mathcal{V}_{n,j,j+1}^z + g\mu_B E_0 c^{-1} \left[\sin(\Omega t) \sum_{n=1,2} \sum_j S_{n,j}^x + \cos(\Omega t) \sum_{n=1,2} \sum_j S_{n,j}^y \right] \\ &= -\alpha \sin(\Omega t) \sum_{n=1,2} \sum_j \mathcal{V}_{n,j,j+1}^z + \beta \left[\sin(\Omega t) \sum_{n=1,2} \sum_j S_{n,j}^x + \cos(\Omega t) \sum_{n=1,2} \sum_j S_{n,j}^y \right]. \end{aligned} \quad (\text{S9})$$

Using these Hamiltonians, we numerically solve their time-dependent Schrödinger equations and compute laser-induced vector chirality. The Ω dependence of time-averaged chirality is summarized in Fig. S3, where $\Delta = 0$. It shows that resonant peak structure appear just below and above $\Omega \sim H$ in both the spin-1 chain and spin- $\frac{1}{2}$ ladder as well as the spin- $\frac{1}{2}$ chain in the main text. These results indicate that the resonant behavior generally takes place in a wide class of 1D Heisenberg-type spin models with antisymmetric ME coupling under static magnetic field.

S3. All optical detection scheme for the laser-driven DM interaction and chirality

In the main text, we explained a detection scheme of the laser-driven DM interaction and spin vector chirality through generating spin current. Here, we explain detection schemes which can be performed solely by an optical setup. For systems with a ferromagnetic order, time-resolved magnetooptical Kerr effect (MOKE) can be used to study the dynamical change of magnetization. Figures S4(a) and (b) show setups for measuring laser-driven DM interaction through Faraday and Kerr effects, respectively. As for the pump, THz laser is preferred since the energy scale of excitations in multiferroic magnets typically corresponds to this frequency region. When we apply a suitable THz circularly (or elliptically) polarized laser to multiferroic ferromagnets, its magnetic order is changed from a uniform ferromagnet to a spiral order due to the dynamical DM interaction. This leads to a decrease of the uniform magnetization. Such demagnetization can be detected through the change in the Faraday or Kerr rotation angle before and after the application of pump laser.

A more direct detection scheme is through directional dichroism [Fig. S4(c)]. This is a magnetooptical phenomenon where the light transmission becomes directionally dependent. As we mentioned above, a noncollinear order is generally expected to emerge when circularly (or elliptically) polarized laser is applied to multiferroic, ferro or antiferromagnets and such a spiral state can lead to directional dichroism [4, 5]. Therefore, observing directional dichroism via probe laser would be a smoking gun experiment for laser-driven DM interaction.

Finally, we discuss how to distinguish phenomena induced by synthetic DM interaction from other laser-driven effects. Varying the laser frequency Ω would provide a way of the distinction. As we mentioned in the main text, since the ME coupling g_{me} is strong within the GHz to THz regime, the synthetic DM interaction cannot emerge in other frequency regimes, e.g., optical regime, while heating effect would not be so sensitive to the laser frequency Ω . A more precise way to distinguish the mechanisms is to change the incident direction of the pump laser. Equation (4) in the main text

$$\mathbf{P} = g_{\text{me}} \mathbf{e}_{12} \times (\mathbf{S}_1 \times \mathbf{S}_2), \quad (\text{S10})$$

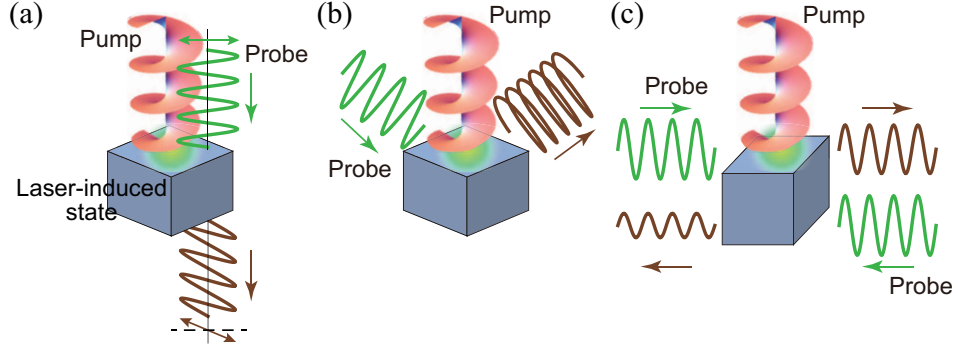


FIG. S4: Schematic images of (a) Faraday effect, (b) Kerr effect, and (c) directional dichroism in the presence of pump laser being circularly polarized. Signatures of laser-driven DM interaction and spin chirality are expected to be detected by measuring these magneto-optical effects.

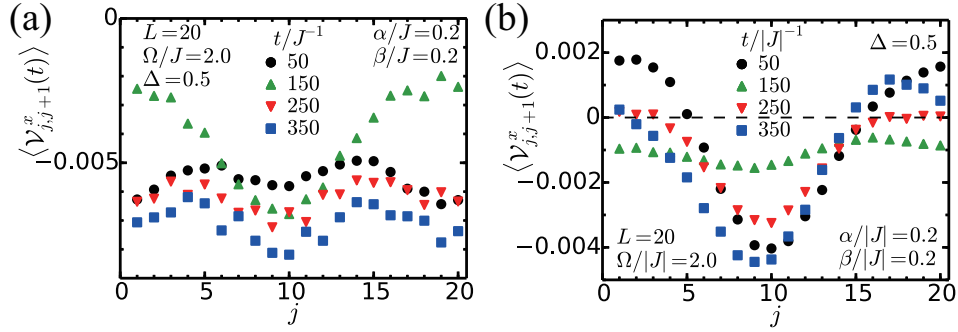


FIG. S5: Time evolution and site dependence of $\langle \mathcal{V}_{j,j+1}^x(t) \rangle$ in (a) AF and (b) ferromagnetic XXZ models under a spatially modulated laser with $\alpha_{j,j+1}$ and β_j .

shows that the ME interaction between polarization and pump laser strongly depends on the geometric relation between the crystal axis $\parallel \mathbf{e}_{12}$ and the laser direction. The strength of laser-driven DM interaction is thereby changed when varying the incident direction of the pump laser and this will be generally different from other laser-driven phenomena including heating effect.

S4. Spatially modulated laser and spin currents

In the final part of the main text, we discussed a way of generating spin current by applying spatially modulated laser which can be induced in near field of chiral plasmonic structures. To confirm that a spatial modulation of the laser results in an inhomogeneous chirality and thus to spin current generation, we perform numerical simulations for multiferroic spin- $\frac{1}{2}$ chains with a spatially modulated laser. The effect of spatial modulation is incorporated by making the field strength parameters α and β site-dependent as

$$\alpha_{j,j+1} = \alpha(\sin^2(\pi j/L) + \sin^2(\pi(j+1)/L))/2, \quad \beta_j = \beta \sin^2(\pi j/L), \quad (\text{S11})$$

respectively. The numerical results are shown in Fig. S5. The driven vector chiralities strongly depend on their site positions, which clearly indicates an emergence of a finite spin current $\langle dS_j^x/dt \rangle$.

-
- [1] C. Kittel, *Introduction to Solid State Physics* (Wiley, New York, 2004).
 - [2] T. Kitagawa, T. Oka, A. Brataas, L. Fu, and E. Demler, *Phys. Rev. B* **84**, 235108 (2011).
 - [3] T. Mikami, S. Kitamura, K. Yasuda, N. Tsuji, T. Oka, and H. Aoki, *Phys. Rev. B* **93**, 144307 (2016).
 - [4] S. Miyahara and N. Furukawa, *J. Phys. Soc. Jpn.* **81**, 023712 (2012).
 - [5] S. Kibayashi, Y. Takahashi, S. Seki, and Y. Tokura, *Nat. Commun.* **5**, 4583 (2014).